Automated Fluorescence Rejection Using Shifted Excitation Raman Difference Spectroscopy

JUN ZHAO,* MIKE M. CARRABBA, and FRITZ S. ALLEN

Chromex, Inc., 2705 Pan American Freeway, NE, Albuquerque, New Mexico 87107

Sample fluorescence is detrimental to Raman spectroscopic analysis. Several algorithms are proposed to achieve automatic fluorescence rejection (AFR) based on shifted excitation Raman difference spectroscopy. The algorithms are mathematically linear and can be automated. The methods are based on a wavelength-tunable laser and the measurement and calibration of both the Raman and the excitation spectra. Applying the AFR methods to highly fluorescent samples significantly reduces the fluorescence background and reveals weak Raman features unidentifiable using traditional methods. Fixed pattern "noise" associated with the background can be completely removed. The merits of each algorithm are discussed and the best excitation frequency shift to perform the analysis is found to be comparable to the widths of major Raman peaks.

Index Headings: **Raman spectroscopy; Fluorescence; Luminescence; Shifted excitation Raman difference spectroscopy; Convolution; Deconvolution; Integral transform; Fourier transform; Dirac delta function; Fixed pattern noise.**

INTRODUCTION

Sample luminescence has been a prohibiting factor for the widespread use of Raman spectroscopy as an analytical technique for a broad range of samples and applications. When present, it often overwhelms the weaker Raman signal and renders the result useless. At least two kinds of luminescence are commonly encountered in Raman spectroscopy, including fluorescence and phosphorescence. In practice, they are both commonly referred to as fluorescence, in spite of the physical origin. Due to its much longer lifetime, phosphorescence may be excited by light of shorter wavelengths, such as room light; the stored energy can be released later when stimulated by a longer wavelength laser beam. As a result, phosphorescence may contain a large portion of emission blue-shifted relative to the Raman excitation. A practical application of this phenomenon is IR viewing cards sensitized with phosphorescent agents. Fluorescence has a lifetime longer than Raman but much shorter than phosphorescence and can be considered instantaneous on the scale of typical Raman integration times. Because fluorescence relies on excited electronic states and fewer samples have chromophores excitable by light of longer wavelength, it is often less problematic when longer wavelength lasers are used. It is largely for this reason that lasers of near-infrared wavelengths are commonly employed in commercial Raman instruments, despite the disadvantage that Raman intensity also drops off as excitation wavelength increases. Currently, 785-nm semi-conductor lasers for dispersive instruments and 1064-nm Nd:YAG lasers for FT-Raman constitute the most popular choices.

Received 19 November 2001; accepted 25 February 2002.

* Author to whom correspondence should be sent.

Several techniques exist to overcome the fluorescence problem. In some cases, Raman can be resonantly enhanced when the excitation matches an absorption band of the analyte, to the extent that it becomes much stronger than the fluorescence. Fluorescence can be quenched when the analyte is adsorbed on some conducting material such as metals and graphitic carbon. Time-resolved Raman utilizes the fact that fluorescence is a longer-lasting effect while Raman is instantaneous. A large portion of the fluorescence can be excluded from the spectrum by using pulsed lasers and limiting signal collection to just the duration of the short pulse. This technique, however, involves sophisticated instrumentation and is not effective when the fluorescence lifetime is comparable to the excitation pulse duration. In the case where the sample is solid and the fluorescence is caused by trace amounts of impurities, sometimes the offending impurity can be destroyed by photobleaching the sample with the excitation laser. A less established method for removing luminescence from Raman measurements is shifted excitation Raman difference spectroscopy (SERDS). First proposed in 1992 by Mathies et al.,[1] the technique requires the acquisition of two spectra excited with slightly different laser frequencies. Assuming the luminescence does not change and the Raman scattering is shifted by the frequency difference of the two excitations, a difference Raman spectrum is obtained by subtracting one spectrum from the other, while the luminescence common to both spectra is removed. The derivative-like difference spectrum is then fitted with the difference of suitable peak shapes, and the result is used to reconstruct the true Raman spectrum free of fluorescence and noise. While this method is effective in removing the luminescence background, because it is based on peak fitting, it is inherently nonlinear, generally not applicable to the analysis of unknown samples, and the resulting Raman spectrum is subject to operator errors. Lieberman et al. proposed a variation of this method, where the excitation frequency was unchanged but the grating was moved slightly to generate a second spectrum of shifted frequency.[2] The data was then processed in the same way as the original method, and as such, it suffers the same shortcomings. In addition, because the luminescence as well as the Raman is shifted, theoretically, it can never be completely removed.

Clearly, spectra of slightly different excitation frequencies contain more information than those acquired with the same excitation frequency. If the luminescence is indeed invariant with excitation frequency shift, then SERDS should be able to remove it and yield clean Raman spectra. What is lacking is an algorithm that is linear, easy to implement, free of human error, and that requires

0003-7028/02/5607-834$2.00/0

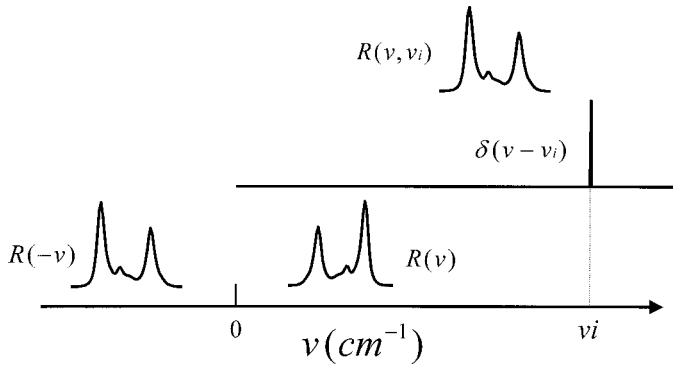

FIG. 1. Illustration of Raman scattering as a convolution process, $R(\nu, \nu_i) = R(-\nu) \otimes \delta(\nu - \nu_i)$.

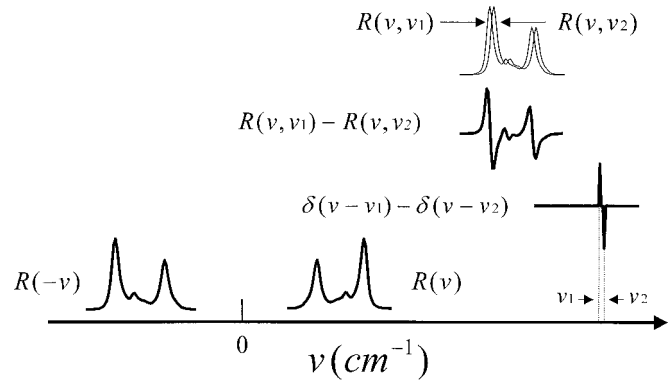

FIG. 2. Illustration of the Difference_Deconvolution method, $R(\nu, \nu_1) - R(\nu, \nu_2) = R(-\nu) \otimes [\delta(\nu - \nu_1) - \delta(\nu - \nu_2)]$.

no prior knowledge other than what is measured by the instrument. The possible form of such algorithms presented as linear deconvolution and integral transforms has been discussed.[3–5] Here, we describe in detail these automatic fluorescence rejection (AFR) algorithms and their implementations. An inexpensive single mode diode laser, whose wavelength is easily selectable by varying the diode temperature, offers the different excitation frequencies. A previously discussed technique allows the simultaneous acquisition and calibration of both the laser and the Raman spectra.[6] The two Raman spectra are subtracted and the resulting derivative-like spectrum yields a true Raman spectrum devoid of luminescence through one of several simple integral transforms.

THEORY

The total signal collected on the detector generally contains Raman, luminescence, and perhaps stray light. The intensity is affected by instrumental parameters such as filter functions, grating efficiency, detector response, etc., and their collective effect is to impose onto the spectrum a shape factor $f(\nu)$, which is a function of the absolute frequency ν only. The $f(\nu)$ of a particular instrument can be calculated by measuring the spectrum of a light source of known spectral characteristics and dividing the true spectrum by the measured one. Thus, the total signal S as a function of absolute frequency ν can be expressed as:

$$S(\nu, \nu_i) = [L(\nu, \nu_i) + R(\nu, \nu_i)]/f(\nu) \quad (1)$$

where $\nu_i = \nu_1, \nu_2$, representing the two excitation frequencies. L and R are the luminescence and the Raman intensities, respectively.

Let's make a few assumptions: (1) both luminescence and Raman intensities are proportional to the excitation intensity I_i; (2) the luminescence term L is invariant with excitation frequency ν_i; (3) the Raman term is simply shifted without intensity change as excitation frequency changes.

Let's first consider the case where the two excitation intensities are equal, such that $I_1 = I_2$. With these assumptions we find:

$$L(\nu, \nu_1) = L(\nu, \nu_2) = L(\nu) \quad (2)$$

$$R(\nu, \nu_1) = R(\nu - \Delta\nu, \nu_2) \quad (3)$$

where $\Delta\nu = \nu_2 - \nu_1$.

We start developing the algorithm by noting that the Raman term, $R(\nu, \nu_i)$, can be expressed as the convolution of $R(-\nu)$, which is the mirror image of the true Raman shift spectrum $R(\nu)$, and the excitation spectrum. For a substantially monochromatic laser beam, the excitation spectrum can be expressed as a Dirac delta function $\delta(\nu - \nu_i)$, hence:

$$R(\nu, \nu_i) = \int R(\nu - \nu')\delta(\nu' - \nu_i)\, d\nu' = R(-\nu) \otimes \delta(\nu - \nu_i) \quad (4)$$

where $\otimes$ denotes convolution. This is illustrated in Fig. 1.

It follows, then, that:

$$\Delta S(\nu) f(\nu) = R(\nu, \nu_1) - R(\nu, \nu_2) = R(-\nu) \otimes [\delta(\nu - \nu_1) - \delta(\nu - \nu_2)] \quad (5)$$

where $\Delta S(\nu) \equiv S(\nu, \nu_1) - S(\nu, \nu_2)$.

Thus, the difference spectrum is simply the true Raman spectrum convolved with the difference of the two delta functions, as shown in Fig. 2. It follows that $R(-\nu)$ can be obtained by deconvolving the difference spectrum with the difference of the two delta functions. We call this method "Difference_Deconvolution". Deconvolution can be carried out using a variety of methods; among them the most basic is using Fourier transformation. Namely, if

$$a = b \otimes c \quad (6)$$

then,

$$b = F^{-1}[F(a)/F(c)] \quad (7)$$

where F denotes forward Fourier transform, and F^{-1} denotes the inverse.

Alternatively, if we integrate the above equation and use the convolution property:

$$\int (a \otimes b) = \left(\int a\right) \otimes b = a \otimes \left(\int b\right) \quad (8)$$

we have,

$$\int \Delta S(\nu) f(\nu)\, d\nu = R(-\nu) \otimes \int [\delta(\nu - \nu_1) - \delta(\nu - \nu_2)]\, d\nu \quad (9)$$

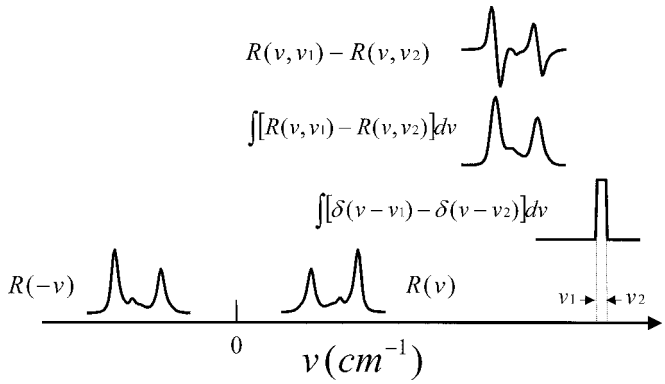

FIG. 3. Illustration of the Boxcar_Deconvolution method, $\int [R(\nu, \nu_1) - R(\nu, \nu_2)]\, d\nu = R(-\nu) \otimes \int [\delta(\nu - \nu_1) - \delta(\nu - \nu_2)]\, d\nu$.

The integral in the above equation is a boxcar function of unit height, with the center at $\bar{\nu} = (\nu_1 + \nu_2)/2$ and a width of $\Delta\nu$:

$$\int [\delta(\nu - \nu_1) - \delta(\nu - \nu_2)]\, d\nu = \begin{cases} 1, & \nu_1 < \nu < \nu_2 \\ 0, & \nu < \nu_1 \quad \text{or} \quad \nu > \nu_2 \end{cases} \tag{10}$$

Therefore, $R(-\nu)$ can be calculated by integrating the difference function and then deconvolving the result with the boxcar function. This is illustrated in Fig. 3. We call this method "Difference-Integration-Boxcar_Deconvolution", or in short, "Boxcar_Deconvolution".

Furthermore, the boxcar function itself of Eq. 10 can be expressed as the convolution of a delta function centered at $\bar{\nu}$ and another boxcar function centered at $\nu = 0$:

$$\int [\delta(\nu - \nu_1) - \delta(\nu - \nu_2)]\, d\nu = \delta(\nu - \bar{\nu}) \otimes \int [\delta(\nu + \Delta\nu/2) - \delta(\nu - \Delta\nu/2)]\, d\nu \tag{11}$$

Thus,

$$\int \Delta S(\nu) f(\nu)\, d\nu = \left\{ R(-\nu) \otimes \int [\delta(\nu + \Delta\nu/2) - \delta(\nu - \Delta\nu/2)]\, d\nu \right\} \otimes \delta(\nu - \bar{\nu}) \tag{12}$$

In arriving at Eq. 12, we have used the commutative and associative properties of convolution.

The term inside the braces is $R(-\nu)$ convoluted with a boxcar function centered at $\nu = 0$ with a width of $\Delta\nu$. When $\Delta\nu$ is small, this term is just $R(-\nu)$ measured with a slightly degraded resolution, i.e., with an instrument of equivalent exit slit width of $\Delta\nu$. If we are content with the slight loss of resolution (and as we shall see, a beneficial enhanced signal-to-noise ratio), then this is all we need. We shall give this term a special name and call it $R_{\Delta\nu}(-\nu)$, thus

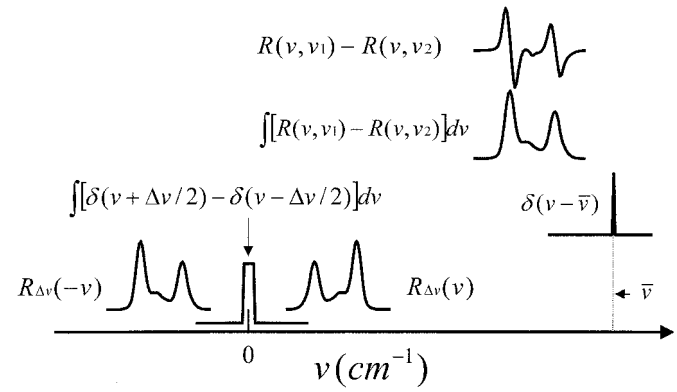

FIG. 4. Illustration of the δ_Deconvolution method, $\int [R(\nu, \nu_1) - R(\nu - \nu_2)]\, d\nu = R_{\Delta\nu}(-\nu) \otimes \delta(\nu - \bar{\nu})$.

$$R_{\Delta\nu}(-\nu) \equiv R(-\nu) \otimes \int [\delta(\nu + \Delta\nu/2) - \delta(\nu - \Delta\nu/2)]\, d\nu \tag{13}$$

$$\int \Delta S(\nu) f(\nu)\, d\nu = R_{\Delta\nu}(-\nu) \otimes \delta(\nu - \bar{\nu}) \tag{14}$$

This relationship is illustrated in Fig. 4.

Therefore, $R_{\Delta\nu}(-\nu)$ can be obtained by deconvolving $\int \Delta S(\nu) f(\nu) d\nu$ with the delta function $\delta(\nu - \bar{\nu})$. This is mathematically equivalent to simply shifting $\int \Delta S(\nu) f(\nu) d\nu$ toward lower frequency by $\bar{\nu}$. The steps required to calculate the broadened Raman shift spectrum are thus very simple, and involve subtraction, integration, and shifting to get $R_{\Delta\nu}(-\nu)$, then mirroring around zero cm^{-1} to get $R_{\Delta\nu}(\nu)$. We call this method "Difference-Integration-δ_Deconvolution", or "δ_Deconvolution", illustrated in Fig. 4.

So far we have concerned ourselves with the case where the two excitation intensities are equal. When this is not true, we must normalize the intensities before carrying out the subtraction. We shall rewrite Eq. 1 as follows:

$$S(\nu, \nu_i) = [l(\nu) + r(\nu, \nu_i)] I_i / f(\nu) \tag{15}$$

where $l(\nu)$ and $r(\nu, \nu_i)$ are the luminescence and Raman spectra excited with unit laser intensity, satisfying the three conditions set forth earlier. Now we normalize against I_1, then:

$$[S(\nu, \nu_1) - (I_1/I_2) S(\nu, \nu_2)] f(\nu) = [r(\nu, \nu_1) - r(\nu, \nu_2)] I_1 \tag{16}$$

Thus, all previous analysis would be valid if we simply add the scaling factor (I_1/I_2) in front of $S(\nu, \nu_2)$.

How do we get the scaling factor (I_1/I_2)? It is not easily measured since these are intensities actually delivered to the sample. It is not necessarily proportional to the output of the excitation source because the optical train can have different throughput for different laser frequencies. But the scaling factor can be calculated from the measurements.

From Eq. 15, we have:

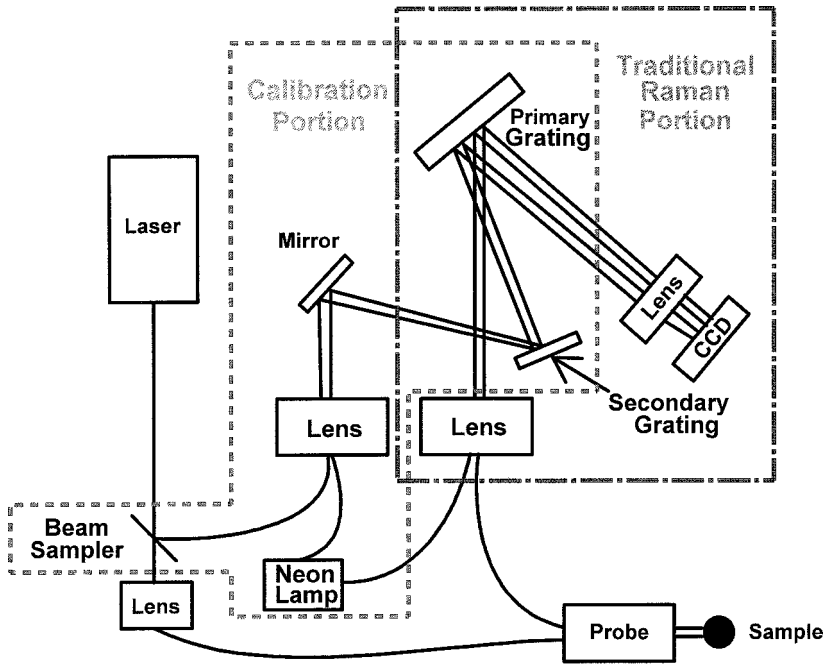

FIG. 5. Schematics of the Sentinel® optical layout.

$$\frac{\int S(\nu, \nu_1) f(\nu)\, d\nu}{\int S(\nu, \nu_2) f(\nu)\, d\nu} = \frac{I_1}{I_2} \frac{\int l(\nu)\, d\nu + \int r(\nu, \nu_1)\, d\nu}{\int l(\nu)\, d\nu + \int r(\nu, \nu_2)\, d\nu} \quad (17)$$

Since

$$\frac{\int l(\nu)\, d\nu}{\int l(\nu)\, d\nu} = \frac{\int r(\nu, \nu_1)\, d\nu}{\int r(\nu, \nu_2)\, d\nu} = 1$$

we have:

$$\frac{I_1}{I_2} = \frac{\int S(\nu, \nu_1) f(\nu)\, d\nu}{\int S(\nu, \nu_2) f(\nu)\, d\nu} \quad (18)$$

Thus, the scaling factor is the ratio of the integrated total signal intensity after correcting for the shape factor. Normalizing the spectra using the integrated intensity guarantees the integrated area of the difference spectrum to be zero, causing the end point of the integrated spectrum also to be zero. In doing so, one must make sure that neither spectrum is saturated on the detector, or the measured result is no longer a true representation of the sample. If saturation does occur, integration time may be shortened or the laser power reduced, and multiple spectra can be coadded to boost SNR.

In the case where the luminescence is much stronger than Raman, we may also use:

$$\frac{I_1}{I_2} = \frac{S(\nu, \nu_1)}{S(\nu, \nu_2)} = \frac{\int S(\nu, \nu_1)\, d\nu}{\int S(\nu, \nu_2)\, d\nu} \quad (19)$$

such that the scaling factor can be calculated before applying for the shape factor.

EXPERIMENTAL

All spectra were acquired on a Chromex Sentinel® Raman spectrometer, a schematic of which is shown in Fig. 5. Algorithms developed here were implemented in Grams Array Basic™ (Galactic Industries). The Sentinel® was equipped with a 785-nm 70 mW diode laser. The laser wavelength was selectable within a 4-nm window, and this was done by changing the diode temperature from the computer. The laser was coupled to an $f/2$ Raman probe, and the Raman signal was carried to the spectrometer through a returning fiber. The spectrograph had the traditional Raman portion, as well as an additional calibration portion to measure and calibrate the laser. All lenses were used on-axis, resulting in excellent imaging quality and minimal point spreading. In addition to the primary grating, a secondary grating was added to further disperse the laser and laser-neon spectrum to achieve higher resolution and wavelength accuracy. The detector was a charge-coupled device (CCD) camera (Andor Technology) with 1024 × 256 pixels, thermoelectrically cooled to −40 °C. The spectrometer collected the Raman and the laser spectra simultaneously, along with their respective calibration spectra from an argon–neon emission lamp. Since there were no ArNe peaks in the vicinity of the 785-nm laser line, the laser beam and its ArNe beam were merged by the means of optical fibers. Thus, altogether, three spectra were collected at the same time, in-

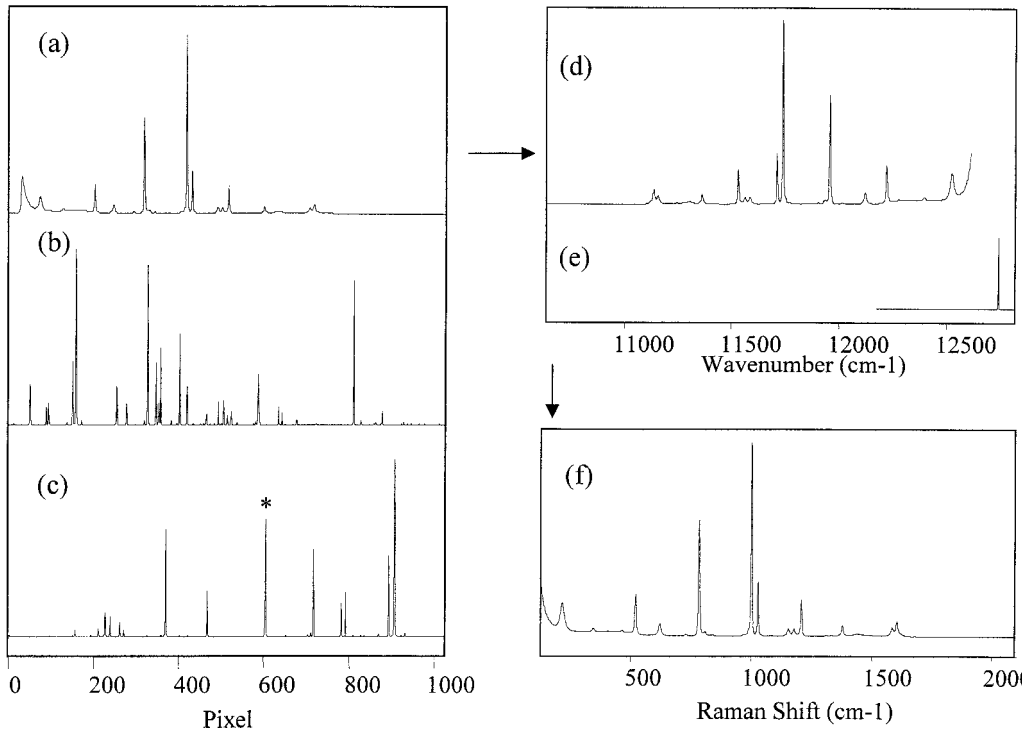

FIG. 6. Illustration of data acquisition and calibration. (**a**) Raw Raman spectrum of toluene; (**b**) neon-argon spectrum used to calibrate Raman; (**c**) laser and neon-argon merged in a single spectrum; the peak indicated by * is the laser; (**d**) Raman spectrum calibrated into absolute wavenumber; (**e**) laser spectrum calibrated into absolute wavenumber; and (**f**) final Raman spectrum in Raman shift.

cluding the Raman, the ArNe for the Raman calibration, and the laser ArNe spectra. These three spectra were focused on different stripes of the CCD to avoid cross talk. The measurement and accurate calibration of both the laser and the Raman are essential to ensure the correctness of SERDS. It is imperative that the Raman channel is free of contamination from the neon and laser light. All spectra were interpolated by a factor of 8 by way of zero filling in the Fourier domain, unless otherwise noted. The Raman spectrum was then calibrated to wavelength by fitting 12 neon and argon emission peaks ranging from 794 to 922 nm with a third-order polynomial. Typical standard deviation of the fitting was below 0.004 nm. The laser was calibrated with five emission peaks ranging from 763 to 801 nm with a second-order polynomial, and typical standard deviation was less than 0.003 nm. The resulting spectra were converted to cm^{-1} with an even point spacing of roughly 0.26 cm^{-1}. In its normal mode of operation, the calibrated Raman spectrum was deconvolved with the laser spectrum to yield the regular Raman shift spectrum, as depicted in Fig. 6. When doing automated SERDS, the final deconvolution step was not done until the two sets of spectra were acquired, calibrated, and subtracted.

The shape factor $f(\nu)$ was measured and applied using a method developed by McCreery et al.,[7,8] with a slight modification. In its original form, this method involves measuring a fluorescence spectrum of a piece of glass on the instrument and calibrating the abscissa into Raman shift. The fluorescence spectrum had previously been characterized, and the shape factor $f(\nu)$ was calculated by dividing $P(RS)$ by the measured fluorescence spectrum, where $P(RS)$ is a sixth-order polynomial in terms of RS, the Raman shift relative to 785-nm excitation.[9] Due to the nature of the algorithms developed here, the shape factor must be applied prior to conversion into Raman shift, and therefore, it was necessary to express the shape factor in terms of absolute wavenumber, ν, instead of Raman shift, RS. This was easily done by substituting $P(RS)$ with $P'(\nu) = P(12738.8 - \nu)$. Because the shape factor was a function of the throughput of the relevant optics and was independent of laser frequency, the same factor can be used for all different excitation frequencies. Furthermore, assuming the fluorescence profile of the glass was invariant with excitation frequency around 785 nm, it was not necessary to set the laser wavelength at 785 nm to measure the fluorescence spectrum.

A luminescent isopropanol sample was prepared by dissolving a trace amount of a laser dye, HITC perchlorate (Exciton, Inc.), in acetone, and then dissolving a small amount of the acetone solution in a large portion of isopropanol in a glass vial. A fluorescent 4-acetamidophenol sample was prepared by mixing 4-acetamidophenol crystalline powder with some ground soil in a glass vial.

To perform automated SERDS, a Raman spectrum was collected from the sample, and then the laser was quickly changed to another frequency by the system computer and a second Raman spectrum was collected with the same integration time, without any change to the sample. All raw spectra reported here were integrated 20 s each.

RESULTS AND DISCUSSION

Figure 7 shows the results of the Difference–Deconvolution method applied to the fluorescent isopropanol spectra. Figure 7a shows the two shape-corrected Raman spectra displayed in absolute wavenumber; their

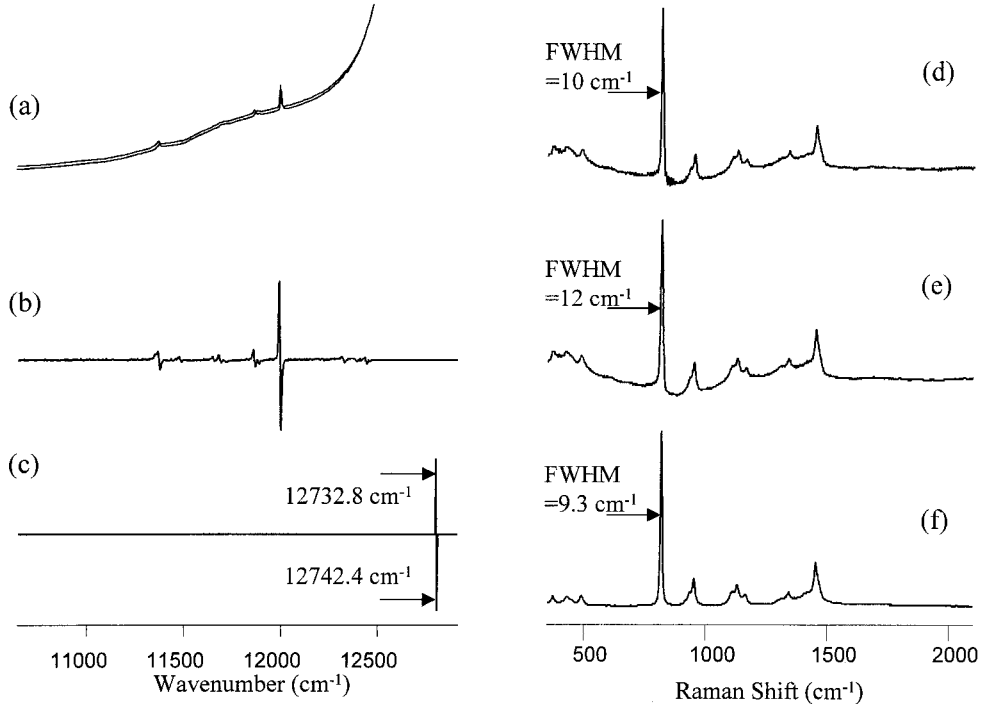

FIG. 7. Implementation of the Difference_Deconvolution method to a fluorescent isopropanol sample. (**a**) The two calibrated and shape-corrected Raman spectra obtained with two different excitation frequencies; (**b**) the Raman difference spectrum; (**c**) the excitation difference spectrum; (**d**) the Raman spectrum obtained by deconvolving (**b**) with (**c**), showing the absence of fluorescence background and some additional side-wing modulations near the major Raman peak; (**e**) the Raman spectrum obtained with the additional step of cosine apodization; and (**f**) the Raman spectrum of pure isopropanol.

excitation frequencies are 12 732.8 and 12 742.4 cm^{-1}, respectively. The underlying fluorescence background masks most of the Raman features except for the major peak. Figure 7b is the difference Raman spectrum, and Fig. 7c is the difference laser spectrum presented as a delta function. As shown in Fig. 7b, the Raman difference appears as a differential form of a spectrum centered at zero intensity, testifying to the validity of the assumptions made earlier. The Raman difference spectrum is extended by zero filling to cover the laser peak positions on the larger wavenumber side, and a direct deconvolution of Fig. 7b with Fig. 7c yields the Raman spectrum in Fig. 7d. Obviously, Fig. 7d is much better in visual appearance than the raw spectra in Fig. 7a, and it is largely free of the fluorescence background plaguing the raw spectra. Comparing Fig. 7d with a pure isopropanol spectrum, Fig. 7f, all the details are revealed and the resolution is roughly the same. However, some artifacts appear as side-wing modulations near the major Raman peak at 820 cm^{-1}, and this is caused by noise magnification during the division in the Fourier domain, as in Eq. 7. Such a phenomenon has been explained in detail in the literature and is intrinsic to the simple linear deconvolution method.[10] However, it can be largely suppressed by apodizing the Fourier transforms prior to the inverse FT. The spectrum in Fig. 7e is the result of applying a cosine apodization function, and it is quite effective in removing the side wings, at the expense of a slight degradation of the resolution, as indicated by the increase of full width at half-maximum (FWHM) of the peak at 820 cm^{-1}.

Figure 8 illustrates the implementation of the two Difference-Integration_Deconvolution methods. Figure 8a is the integration of Fig. 7b, and Fig. 8b is the integration of Fig. 7c. Directly deconvolving Fig. 8a with the boxcar function in Fig. 8b yields the Raman spectrum shown in Fig. 8d. Again, side-wing modulations are present and apodization improves the situation at the expense of resolution, as shown in Fig. 8e. Thus the Boxcar_Deconvolution method is similar to the Difference_Deconvolution method, as one is derived from the other. Figure 8c shows the excitation spectrum represented by a δ function centered at the average laser frequency 12 737.6 cm^{-1}, and deconvolving Fig. 8a with Fig. 8c yields Fig. 8f, which is free of any undesirable modulations, but at an even greater expense of spectral resolution.

Given a widely tunable excitation source, how does the frequency shift $\Delta\nu$ affect the spectral properties, or what is an appropriate value for $\Delta\nu$ for a given system? The impact of $\Delta\nu$ on the fluorescent isopropanol spectra is exhibited in Figs. 9 through 11 for the three algorithms, where $\Delta\nu$ is progressively increased from 1.5 cm^{-1} in the ***a*** spectra to 26.8 cm^{-1} in the ***d*** spectra. For the Difference_Deconvolution method, as shown in Fig. 9, as well as for the Boxcar_Deconvolution method, shown in Fig. 10, increasing $\Delta\nu$ much beyond the FWHM of major Raman peaks results in increased modulation noise. This is expected because $\Delta\nu$ directly limits the bandwidth of the excitation function in the Fourier (frequency) domain, and trying to recover frequency components beyond this limit will amplify noise for higher-frequency components. The greater $\Delta\nu$ is, the lower the band limit is in its Fourier transform, and the lower the modulation frequency, as evidenced in Figs. 9 and 10. On the other hand, decreasing $\Delta\nu$ to much less than the FWHM of major Raman peaks reduces the SNR by diminishing the signal strength, to the extreme where $\Delta\nu = 0$ and the

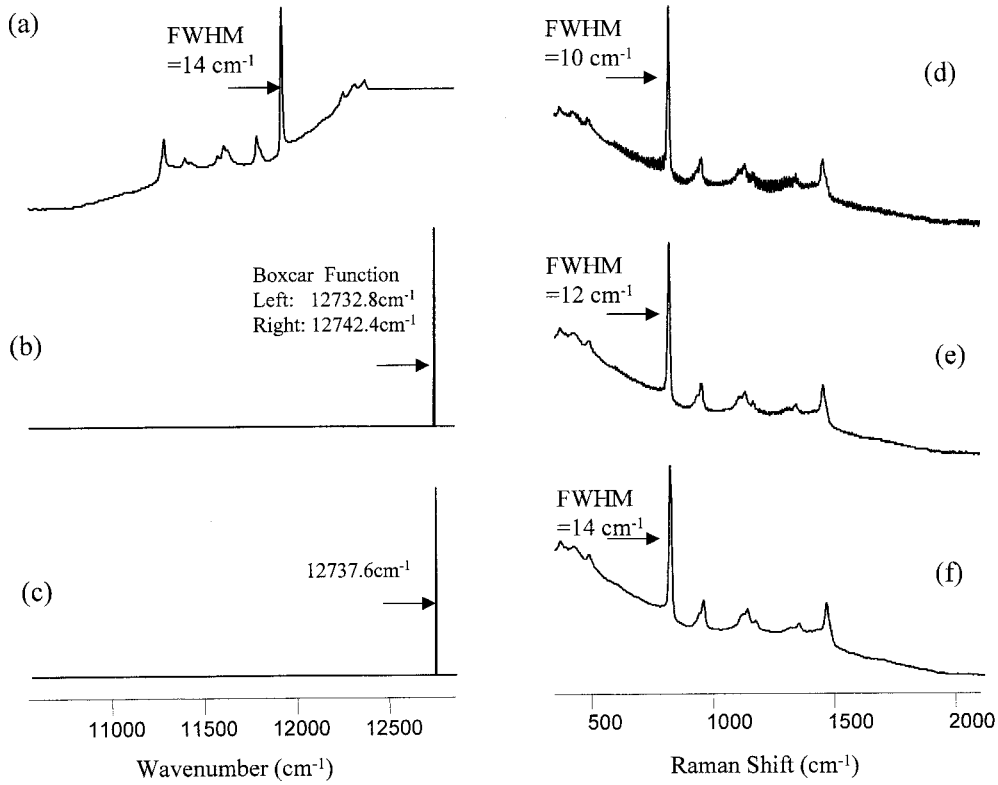

FIG. 8. Implementation of the Boxcar_Deconvolution and the δ_Deconvolution methods to a fluorescent isopropanol sample. (**a**) The integrated Raman difference spectrum obtained by integration of the Raman difference spectrum in Fig. 7b; (**b**) the boxcar function obtained by integrating the excitation difference spectrum in Fig. 7c; (**c**) excitation spectrum represented as a δ-function; (**d**) the Raman spectrum obtained by deconvolving (**a**) with (**b**), showing the absence of fluorescence background and additional baseline modulations; (**e**) the Raman spectrum obtained by deconvolving (**a**) with (**b**), with the additional step of cosine apodization; and (**f**) the Raman spectrum obtained by deconvolving (**a**) with (**c**).

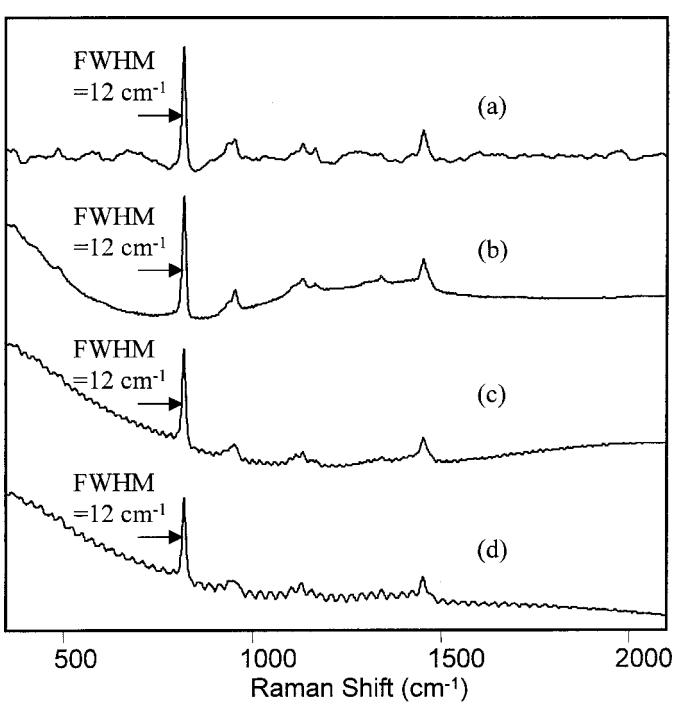

FIG. 9. The effect of excitation frequency shift $\Delta\nu$ on the Difference_Deconvolution method. (**a**) $\Delta\nu$ = 1.5 cm^{-1}; (**b**) $\Delta\nu$ = 9.6 cm^{-1}; (**c**) $\Delta\nu$ = 20.8 cm^{-1}; and (**d**) $\Delta\nu$ = 26.8 cm^{-1}.

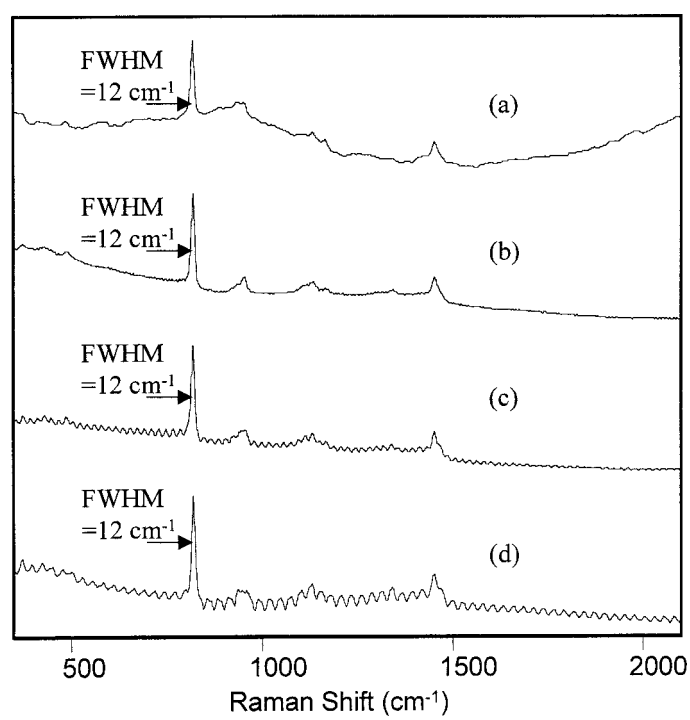

FIG. 10. The effect of excitation frequency shift $\Delta\nu$ on the Boxcar_Deconvolution method. (**a**) $\Delta\nu$ = 1.5 cm^{-1}; (**b**) $\Delta\nu$ = 9.6 cm^{-1}; (**c**) $\Delta\nu$ = 20.8 cm^{-1}; and (**d**) $\Delta\nu$ = 26.8 cm^{-1}.

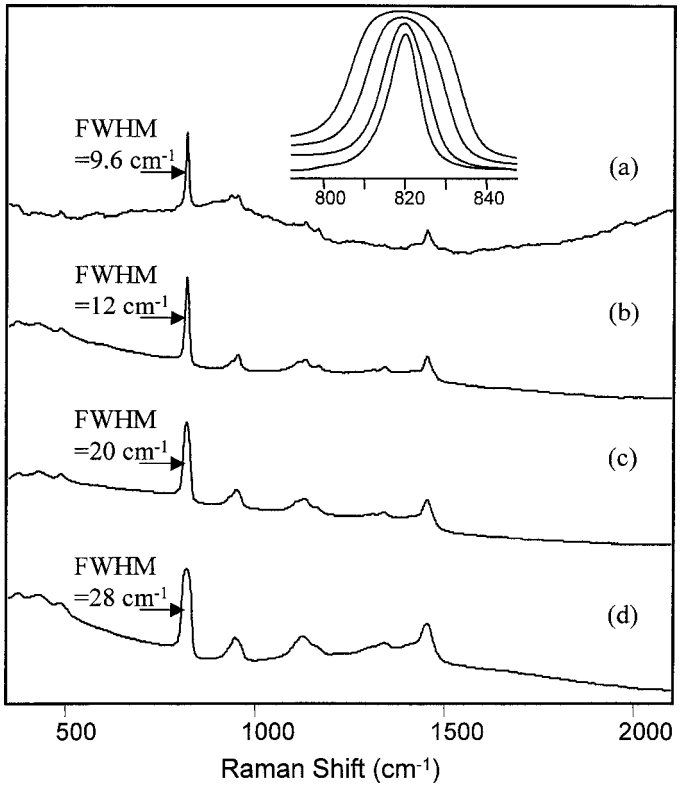

FIG. 11. The effect of excitation frequency shift $\Delta\nu$ on the δ_Deconvolution method. (**a**) $\Delta\nu$ = 1.5 cm^{-1}; (**b**) $\Delta\nu$ = 9.6 cm^{-1}; (**c**) $\Delta\nu$ = 20.8 cm^{-1}; and (**d**) $\Delta\nu$ = 26.8 cm^{-1}. Upper trace, an expanded view of the Raman peak at 820 cm^{-1}.

difference spectrum would contain no Raman signal, and hence no Raman peak would be recovered in the result. Resolution as represented by final FWHM is unaffected by $\Delta\nu$. An appropriate $\Delta\nu$ will yield optimum SNR without significant baseline modulations, and based on the band limit argument, it should be in the neighborhood of the smallest FWHM of major Raman peaks.

In contrast, the δ_Deconvolution method, as shown in Fig. 11, produces no side-wing modulations; while the apparent SNR improves, the resolution gets progressively worse as $\Delta\nu$ increases, as this algorithm does not try to recover the lost resolution. An expanded view of the 820-cm^{-1} peak is shown in the upper trace, where the peak intensities are normalized and the baseline offset for comparison. From inside out, the peaks represent those in spectra ***a*** through ***d,*** respectively. The peak shape is visibly distorted in ***c*** and ***d,*** and it becomes more like a square wave as $\Delta\nu$ gets very large. The effect is analogous to putting an exit slit of spectral width $\Delta\nu$ and a single detector after the slit and recording the spectrum by scanning the slit across the focal plane. The larger $\Delta\nu$ is, the more signal the detector can gather. Too small a $\Delta\nu$ results in poor signal strength, and increasing $\Delta\nu$ much beyond the FWHM of spectral features distorts the peaks to more like square waves with no benefit in SNR. Optimal results can be obtained when $\Delta\nu$ approximates the original FWHM of the narrowest peak needed to be resolved.

It is of interest to compare the AFR methods developed here with simple baseline subtraction. Bear in mind that simple baseline subtraction performed on a single spectrum involves guessing based on trend, so it is never an accurate solution. This is because only one sum of the Raman and fluorescence is measured, while there are two independent variables, as expressed in Eq. 1. With SERDS, however, there are two independent equations supplied by two raw spectra, so an analytical solution can be found. Figure 12 shows the spectra of a fluorescent sample of 4-acetamidophenol mixed with some backyard soil. Figure 12a shows the two raw spectra, acquired with ν_1 = 12 743.92 cm^{-1} and ν_2 = 12 751.58 cm^{-1}, and thus $\Delta\nu$ = 7.66 cm^{-1}. Figure 12b shows the two shape-corrected spectra. Figure 12c is the Raman difference spectrum and Fig. 12f is the Raman spectrum obtained from Fig. 12c using the Difference_Deconvolution method. There is an undesirable background in Fig. 12f and this is caused by the residual non-zero baseline in Fig. 12c. Applying a multipoint baseline subtraction to Fig. 12c yields Fig. 12d, which has less residual background, and applying the Difference_Deconvolution method to Fig. 12d results in Fig. 12g. Comparing Figs. 12f and 12g with the pure 4-acetamidophenol spectrum in Fig. 12h shows that all the Raman features are recovered by the fluorescence rejection method. In comparison, Fig. 12e is the spectrum derived from one of the spectra in Fig. 12b by multipoint baseline subtraction on a best effort basis. It is evident that Fig. 12e is much noisier than either Figs. 12f or 12g, and most of the weak Raman peaks are buried in the residual background. More explanation will follow. For perspective, in the spectra of Fig. 12b, the 651.9 cm^{-1} Raman peak height is 0.6% of background intensity and the one at 504 cm^{-1} is only 0.1%. The ability to recover very weak Raman signal from intense fluorescence background should be a significant advantage.

Some of the recovering ability can be attributed to the removal of fixed pattern ''noise''. This is demonstrated in Fig. 13. Shown in Fig. 13a are two raw spectra of the same fluorescent 4-acetamidophenol sample acquired with the same excitation frequencies as in Fig. 12a. The spectra are not calibrated or shape corrected. They are acquired with a probe that has two laser rejection interference filters used in series. In addition to the sloping background, and some very weak Raman features, which shift with the excitation frequency, we see fringe patterns that are stationary and well overlapped. In this case the patterns are caused by the etalon effect of the laser rejection filters in the probe, which is deliberately magnified by using two filters in series. These patterns are really not noise, but are throughput variations of the filters. They appear as noise only because the modulation periods are comparable to the pixel spacing of the CCD. They have different characteristics than real noise because they are often linearly proportional to the signal level, such that increasing signal level does not improve apparent SNR. In the region shown, the modulation depth of the fringes, as measured by the peak-to-peak intensity relative to the mean value, is about 1.8%. The same patterns also appear in the fluorescent glass spectrum in Fig. 13b, which is used to calculate the shape factor. In a broadband spectrum such as Fig. 13b, the fringes can be removed by way of smoothing without affecting the overall shape. Figure 13c is the result of removing the high-frequency component from Fig. 13b using Fourier transform. Since the same patterns appear in Fig. 13b, it is

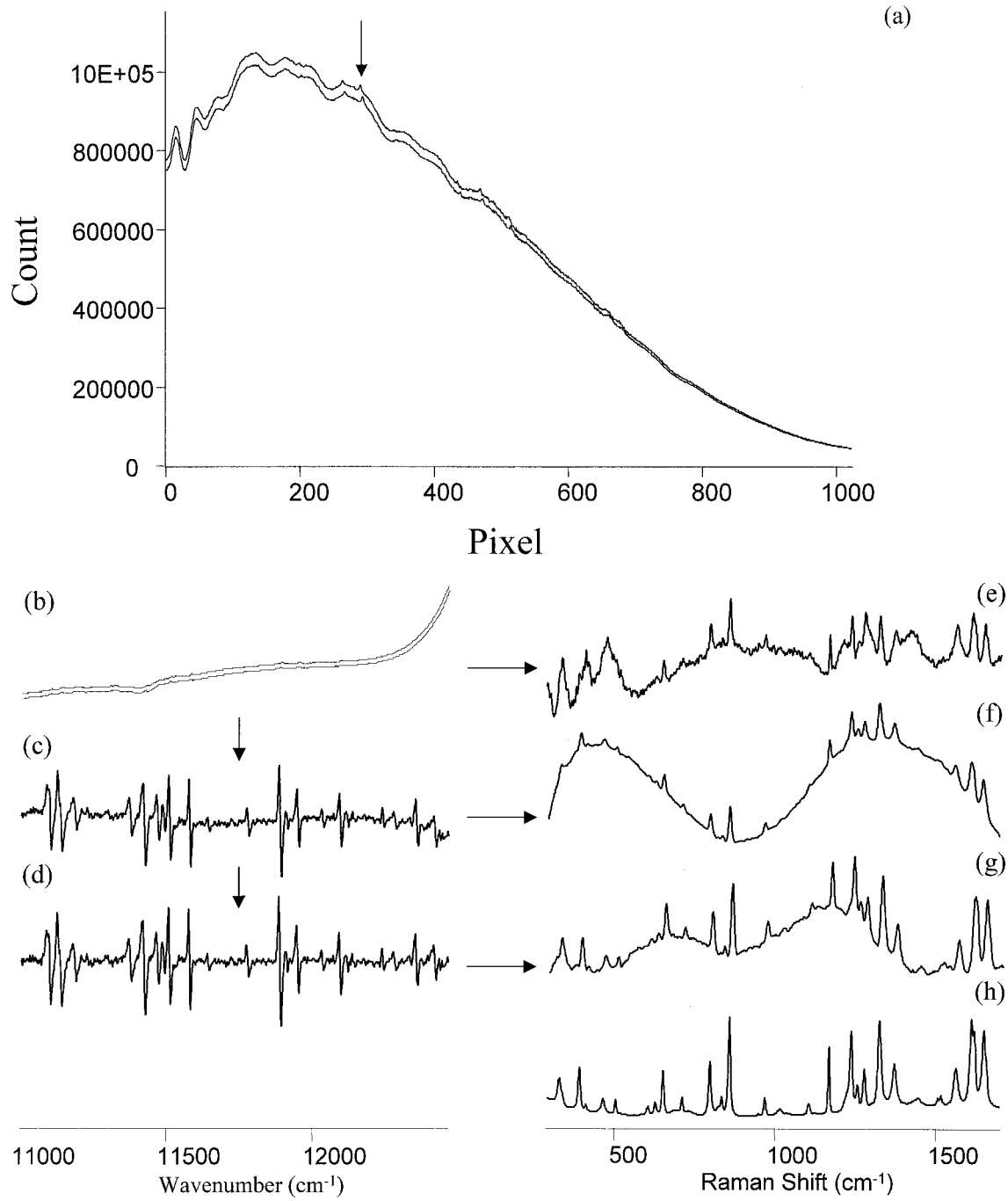

FIG. 12. Comparison of the automated fluorescence rejection method with simple multipoint baseline subtraction. (**a**) The two raw spectra of a fluorescent 4-acetamidophenol sample obtained with two different excitation frequencies, plotted in full scale. The peaks indicated by the arrow correspond to the major Raman peak at 857.9 cm^{-1}; (**b**) the two calibrated and shape-corrected Raman spectra; (**c**) the Raman difference spectrum; (**d**) the Raman difference spectrum obtained via multipoint baseline subtraction from (**c**); (**e**) the Raman spectrum obtained via multipoint baseline subtraction from one of the spectra in (**b**); (**f**) the Raman spectrum obtained from (**c**) using the Difference_Deconvolution method; (**g**) the Raman spectrum obtained from (**d**) using the Difference_Deconvolution method; and (**h**) Raman spectrum of pure 4-acetamidophenol.

possible to correct for these variations by applying the shape factor derived from Fig. 13b. Doing so results in Fig. 13d, where much of the variations indeed disappeared, and Fig. 13h is the Raman spectrum obtained from one of two spectra in Fig. 13d after a multipoint baseline subtraction. If Fig. 13c is used to calculate the shape factor, the resulting spectra are Figs. 13e and 13i. Figure 13i appears noisier than Fig. 13h because the fringe patterns are not corrected in Fig. 13i. The true noise can be calculated by subtracting two successive measurements under the same condition, and the noise level can be taken as the standard deviation of the data near the peak of interest divided by $2^{1/2}$. For the peak at 1278 cm^{-1}, the SNR calculated in this way is about 30. It is evident that the apparent SNR of Fig. 13i is much less than 30, as the main ''noise'' contribution is the fixed pattern ''noise''. Applying the δ_Deconvolution method to Fig. 13e results in Figs. 13f, 13g, and 13j, successively.

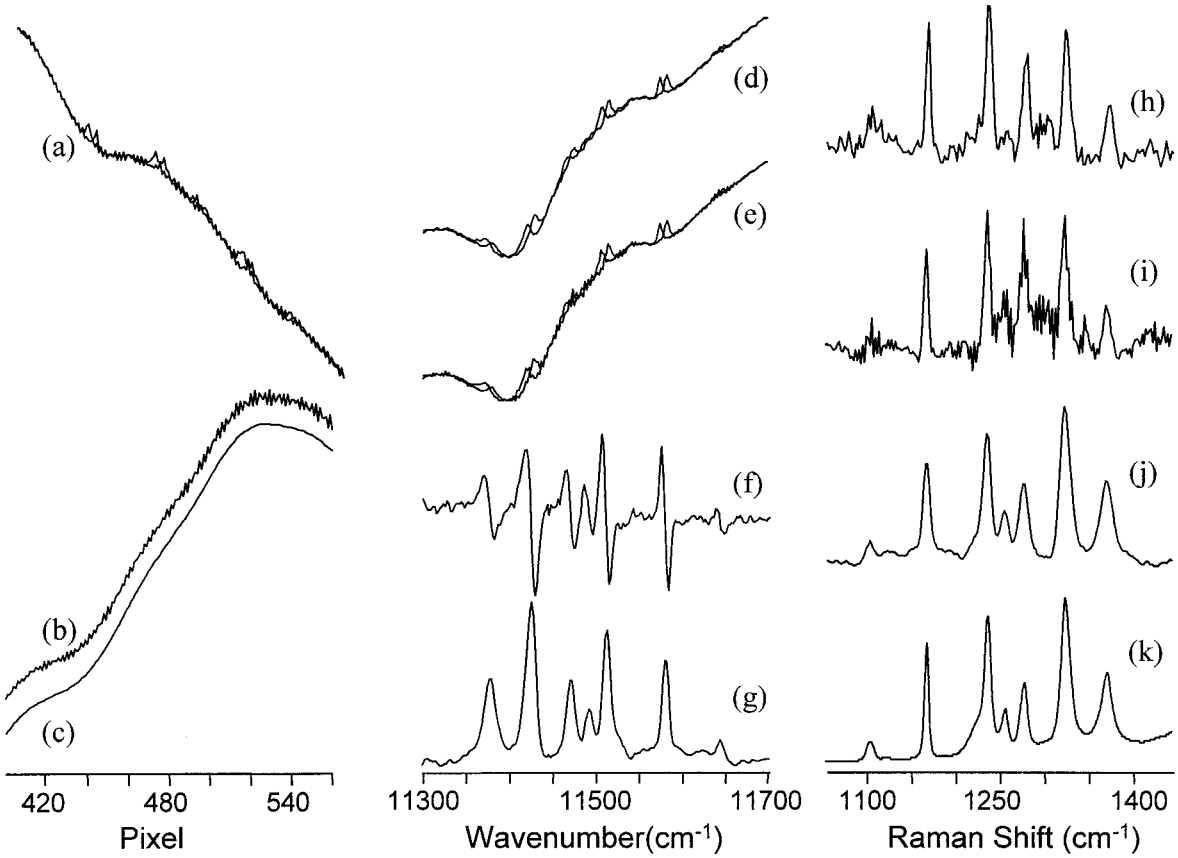

FIG. 13. Removal of fixed pattern ''noise'' using Raman difference. (**a**) A portion of the overlap of two raw Raman spectra of the fluorescent 4-acetamidophenol sample obtained with two different excitation frequencies; (**b**) the broadband spectrum of the fluorescent glass used to derive the shape factor; (**c**) result obtained via Fourier smoothing of (**b**); (**d**) spectra in (**a**) after calibration and shape correction with (**b**); (**e**) spectra in (**a**) after calibration and shape correction with (**c**); (**f**) Raman difference spectrum obtained from (**e**); (**g**) integration of (**f**); (**h**) Raman spectrum obtained via multipoint baseline subtraction from one of the spectra in (**d**); (**i**) Raman spectrum obtained via multipoint baseline subtraction from one of the spectra in (**e**); (**j**) result of δ_Deconvolution from (**g**); and (**k**) pure 4-acetamidophenol spectrum.

Even though the original spectra in Fig. 13e are not corrected for the fringe patterns, the resulting Raman spectrum in Fig. 13j is much better in terms of SNR than either Figs. 13h or 13i, in reference to the pure 4-acetamidophenol spectrum in Fig. 13k. This is advantageous because it means in order to remove the fixed pattern ''noise'' due to the fluorescence background using the methods developed here, the broadband reference spectrum does not have to contain the same fixed pattern ''noise'' as the data. None of the spectra in Fig. 13 are 8× interpolated, in order to show the fringe patterns more clearly.

Fringe patterns can also arise from the detector in back-illuminated CCD cameras. Other factors, such as nonuniform detector response or hot or cold pixels, can also cause fixed pattern ''noise''. Response nonuniformity is common to multichannel detectors since it is impossible to make every sensor element exactly the same. It is also more difficult to identify because it generally lacks patterns. In scientific grade CCDs this is controlled to some small values, typically well below 1%. These small imperfections pose little problem to Raman spectra without much fluorescence background. However, when the fluorescence background is overwhelmingly high, a small percentage of that transforms to large ''noise'' compared with the small Raman features. As illustrated, to some extent, these variations can be corrected by dividing the spectra by that of a smooth broadband source, such as the fluorescent glass used here. However, for complete correction, the reference broadband spectra must contain exactly the same patterns as the sample florescence. This requirement is difficult, if not impossible, to fulfill, because the reference broadband spectra, be it from a white light source or a luminescent glass, comes from a source different than the Raman sample. Small variations such as detector position and temperature can cause the high-pitched patterns to change, while reference sample location, sample absorption, laser penetration depth, and angular distribution of intensity can all affect lower-frequency modulations. The less-than-perfect correction explains the residual low-frequency modulations below 500 cm^{-1} and between 1100 and 1500 cm^{-1} in Fig. 12e. Because applying correction using a reference spectrum containing ''noise'' of different patterns than the data may exacerbate the problem, even in a fixed grating instrument the reference broadband spectrum may have to be re-acquired frequently to assure validity. Because the difference Raman method utilizes two similar spectra of the same sample and subtracts out their common component, including both high-pitched pattern ''noise'' and low-frequency modulations due to the fluorescence background, it can eliminate these artifacts without requiring their exact duplication in the shape factor. Thus, the same shape factor can be used without worrying about changes

in the fixed patterns. This is partly responsible for the better performance of the AFR method than the method of shape correction followed by simple baseline subtraction. It should be noted that the fixed pattern ''noise'' due to the Raman signal itself (instead of the background) is typically much smaller and rarely noticed, such as in Fig. 13k.

It is worth pointing out that true white noise can not be eliminated by any data processing method without affecting the integrity of the signal. Shot noise accompanying all Raman measurements is a white noise; therefore, it is not expected to be removed by the AFR methods proposed here. Given that no treatment of shot noise is attempted, the AFR methods should be neither positively nor negatively affected by it. The enhanced apparent SNR of the processed spectra is caused by the elimination of fixed pattern ''noise'', as well as by the doubled integration time associated with the acquisition of two spectra. For the δ_Deconvolution method, an additional smoothing effect hidden in the algorithm further enhances the appearance, as the final result is the convolution of the true Raman spectrum with a boxcar function. Similar effect can be achieved by convolving a noisy spectrum with a boxcar function, with the same penalty of loss in apparent resolution. Stated differently, the AFR methods do not change the information content of the two original raw spectra; they only make the information more evident. Nonetheless, two spectra excited by two different wavelengths do contain more information than either one.

The frequency accuracy of the various algorithms can be assessed by comparing the Raman peak positions in the spectrum shown in Fig. 12g (obtained via the Difference_Deconvolution method) with their true Raman shift provided by ASTM standards.[11] This is shown in the first three rows in Table I, with the second row being the standard deviation of the ASTM measurements. The measured values are obtained by automatic peak picking in Grams software. Applying the other two methods to the spectrum in Fig. 12d yields the values in rows 4 and 5. As shown, all three methods yield similar results, and most of the peak positions agree with the ASTM standard values within the standard deviation of the ASTM standard, testifying to the good accuracy of all three algorithms.

All three algorithms presented calculate the Raman spectrum directly from the Raman difference spectrum. Theoretically, one can also calculate the fluorescence background first and subtract it out to obtain the Raman spectrum. This would involve shifting one of the two spectra by $\Delta\nu$ such that the Raman features in the two spectra match. Subtracting one from the other would yield a fluorescence difference spectrum, of the form $L(\nu - \Delta\nu) - L(\nu)$, similar to the Raman difference. One can then use the same algorithms developed here to calculate the luminescence spectrum $L(\nu)$.

One remaining issue is the residual background in the Raman difference spectrum, as shown in Fig. 12c. Although it is miniscule compared to the original background, at about 0.2%, it causes a large background in the final Raman spectrum as shown in Fig. 12f. It is not clear what caused the incomplete subtraction, but a possible cause could be small variations in fluorescence pro-

TABLE I. Frequency accuracy of the various fluorescence rejection algorithms assessed by comparing the ASTM standards with the measured positions of major Raman peaks in the fluorescent 4-acetamidophenol spectra. All values in cm^{-1}.

ASTM[a]	329.2	390.9	465.1	504	651.6	710.8	797.2	834.5	857.9	968.7	1168.5	1236.8	1278.5	1323.9	1371.5	1561.5	1648.4
ASTM STD[a]	0.52	0.76	0.3	0.6	0.5	0.68	0.48	0.46	0.5	0.6	0.65	0.46	0.45	0.46	0.11	0.52	0.5
Difference_Deconvolution	328.9	391.8	465	504.7	651.8	711.3	797.3	834.3	858.1	968.6	1168.5	1236.8	1277.8	1323.9	1371.1	1561.6	1648.6
δ_Deconvolution	329.1	392.1	465	504.7	651.8	711.6	797.5	834.1	858.2	968.6	1168.6	1237	1277.8	1324	1371.1	1561.7	1648.7
Boxcar_Deconvolution	328.9	391.8	465	504.7	651.7	711.3	797.3	834.2	858.1	968.6	1168.5	1236.8	1277.8	1323.9	1371	1561.5	1648.5

[a] See Ref. 11.

file when excitation frequency changes. Mathematical routines may be developed to remove such residual background automatically, and it is the subject of future investigations. However, even without such improvements, the data quality after fluorescence rejection is already much better than the original data.

In summary, we have proposed several methods of rejecting fluorescence background in Raman spectroscopy, based on Raman difference spectroscopy using shifted excitations. The Difference_Deconvolution and the Boxcar_Deconvolution methods are similar and can recover spectral resolution while perhaps introducing deconvolution artifacts. Apodization in the Fourier transform reduces such artifacts at the expense of spectral resolution. The δ_Deconvolution method does not recover resolution and yields the best SNR. For all three methods, the best result is obtained when the excitation frequency shift is comparable to the widths of major Raman peaks. Too little shift results in poor SNR, while too much shift results in increased deconvolution artifacts or peak shape distortions. All measurements and data manipulations can be automated without user intervention. The procedures are linear and hence introduce minimal artifacts because all the mathematical steps are linear transforms, including integration and deconvolution. All the methods can substantially suppress the fluorescence background and improve spectral quality. They can remove fixed pattern ''noise'' associated with the background and render visible weak Raman features that are masked by the fluorescence background in the original spectrum. This should expand the utility of Raman spectroscopy to include many samples that are currently difficult to analyze due to fluorescence interference.

1. A. P. Shreve, N. J. Cherepy, and R. A. Mathies, Appl. Spectrosc. **46,** 707 (1992).
2. P. A. Mosier-Boss, S. H. Libberman, and R. Newberry, Appl. Spectrosc. **49,** 630 (1995).
3. F. S. Allen, J. Zhao, and M. M. Carrabba, Abstract 1284, PittCon 2001, New Orleans, LA (2001).
4. J. Zhao, F. S. Allen, and M. M. Carrabba, Abstract 471, 28th Annual FACCS, Detroit, MI (2001).
5. F. S. Allen and J. Zhao, U.S. Patent 6,281,971 B1 (2001).
6. F. S. Allen, J. Zhao, and D. S. Butterfield, U.S. Patent 6,141,095 (2000).
7. K. G. Ray and R. L. McCreery, Appl. Spectrosc. **51,** 108 (1997).
8. K. J. Frost and R. L. McCreery, Appl. Spectrosc. **52,** 1614 (1998).
9. R. L. McCreery, private communication (2001).
10. P. A. Jansson, ''Traditional Linear Deconvolution Method'', in *Deconvolution of Images and Spectra,* P. A. Jansson, Ed. (Academic Press, San Deigo, London, Boston, New York, Sydney, Tokyo, Toronto, 1997), 2nd ed.
11. ''Guide for Raman Shift Standards for Spectrometer Calibration'', in *Annual Book of ASTM Standards,* E1840-96, vol. 3.06 (ASTM, West Conshohocken, PA, 1996).